



Degradation mechanism of LiCoO₂/mesocarbon microbeads battery based on accelerated aging tests



Ting Guan, Pengjian Zuo, Shun Sun, Chunyu Du, Lingling Zhang, Yingzhi Cui, Lijie Yang, Yunzhi Gao*, Geping Yin*, Fuping Wang

Institute of Advanced Chemical Power Sources, School of Chemical Engineering and Technology, Harbin Institute of Technology, Harbin 150001, China

HIGHLIGHTS

- Accelerated cycling tests in a long-term shallow charge and discharge process.
- The degradation mechanism of the LiCoO₂/MCMB full cell is proposed.
- The percentage of each aging factor is calculated.
- The accelerated rate range ensuring no changes in aging mechanism is found out.

ARTICLE INFO

Article history:

Received 5 May 2014

Received in revised form

18 June 2014

Accepted 20 June 2014

Available online 7 July 2014

Keywords:

Accelerated cycling test

Long-term cycle

Cell imbalance

Cathode fade

Active lithium

Polarization

ABSTRACT

A series of LiCoO₂/mesocarbon microbeads (MCMB) commercial cells cycled at different rates (0.6C, 1.2C, 1.5C, 1.8C, 2.4C and 3.0C) are disassembled and the capacity fade mechanism is proposed by analyzing the structure, morphology and electrochemical performance evolution at the capacity retention of 95%, 90%, 85%, 80%. The capacity deterioration of the commercial cell is mainly caused by the decay of the reversible capacity of LiCoO₂ cathode, the irreversible loss of active lithium and the lithium remaining in anode. The proportions of effects by the above three factors are calculated accurately. The consumption of the active lithium leads to a cell imbalance between the anode and the cathode. The electrochemical test results indicate that the capacity fade of the active materials at the low rate is more obvious than that at the high rate. The influence of the active lithium is gradually increscent with the increasing rate. The rate of 1.5C is the optimal value to accelerate the aging of the full cell by comparing the testing results at different capacity retentions in the specific condition of low charge/discharge rate and shallow depth of discharge.

© 2014 Elsevier B.V. All rights reserved.

1. Introduction

Lithium-ion batteries are considered the most promising power sources for electric transportation [e.g., electric vehicles (EVs) and hybrid electric vehicles (HEVs)], portable electronics and so on due to their high energy and power densities. A significant barrier that limits wide-spread commercialization of this technology is the requirement of long battery life, up to 15 years, in a hard environmental condition [1]. As most of the battery

systems, lithium-ion batteries suffer capacity and power fade during both cycling and storage. It is necessary to understand the battery lifetime of the specific applications for safe handing. Knowing the degradation mechanism clearly is favorable to improve the battery performance. In order to estimate the lifetime of the lithium-ion batteries, lifetime prediction under real operation conditions is a key issue for a reliable integration. However, aging tests using real operation conditions are very time and cost intensive, short-term accelerated aging tests are discussed to be a powerful method.

Accelerated aging tests generally conclude storage tests and cycling tests. In the accelerated aging storage tests, cells which are in float condition (constant voltage) or in the open circuit condition are usually stored at different ambient temperatures (usually less than 65 °C) and at different state of charge (SOC). The aging test

* Corresponding authors. School of Chemical Engineering and Technology, Harbin Institute of Technology, No. 92, West Dazhi Street, Harbin 150001, China. Tel.: +86 451 86413721; fax: +86 451 86403807.

E-mail addresses: gao_yunzhihit@hit.edu.cn (Y. Gao), yingphit@hit.edu.cn (G. Yin).

results show that the temperature and the SOC both have effects on the stored cells, especially the temperature. At high ambient temperature or at high SOC, the decay rate of the stored cells is fast [2–9]. Accelerated aging cycling tests usually contain the following stress factors: charge rate, discharge rate, charge/discharge rate, depth of discharge (DOD), charge cut-off voltage and static thermal stress [10–12]. In all systems, the formation and development of an irreversible solid electrolyte interface (SEI) film at the anode is the main cause of the decrease in capacity of the cell [13–17]. Besides, the other side reactions also consume active lithium. The loss of active lithium is suggested to be an important cause of the fade in full cells [18–22]. Furthermore, the imbalance of the cell caused by the irreversible consumption of the active lithium is another important reason leading to the decay of the full cell [23–28]. The structural degradation and the increased resistance induced by particle isolation, electrode delamination, loss of electrical contact within the porous electrode and passive films at the active particle surface also result in the degradation [15,29–32].

To date, although the research about the degradation mechanism of lithium-ion batteries is extensive and in-depth, few is known about the similarities and differences of degradation mechanism under different accelerated aging tests, especially the critical stress factor for a special application condition. In the literatures, they use various accelerated aging tests to shorten the test time. However, the validity of the acceleration method is little discussed. They do not verify whether the methods they used are effective, that is to say, it should be ensured that the method will not change the aging mechanism compared to the real tests. So, it is necessary to investigate the degradation mechanism under different accelerated aging tests for building a set of rational acceleration methods.

In this study, we have investigated the cycling accelerated aging effects on the performance of commercial LiCoO₂/mesocarbon microbeads (MCMB) cells. The capacity fade of cells was studied, and the effects of accelerated charge and discharge rate were analyzed. The structure and surface morphology of both electrodes obtained from dismantled cells before and after cycling were investigated by X-ray diffraction (XRD) and scanning electron microscopy (SEM), respectively. Electrochemical tests on Li/LiCoO₂ and Li/MCMB half-cells were also conducted. The study focused on the questions about the intrinsic performance of each electrode and the cell imbalance at different test rates. If the aging related changes were very similar, it could be assumed that the aging mechanism of full cells fading to the same extent at different test rates was unchanged. So the accelerated rate range which ensured no changes in the degradation mechanisms of the cells could be found out by comparing aging processes of full cells at a series of test rates.

2. Experimental

The commercial prismatic lithium ion batteries (CP475148A cell) which were designed for capacity-type applications were used in this study. These cells consist of LiCoO₂ cathode and MCMB anode with a normal capacity rating of 1.15 Ah and cell dimensions of 47.80 mm long, 50.80 mm wide and 4.70 mm thick. Extended accelerated aging cycling tests have been performed under different charge/discharge rates which varied from 0.6C to 3.0C (0.6C, 1.2C, 1.5C, 1.8C, 2.4C, 3.0C). Before the accelerated tests, the capacities of all cells were determined by a 0.6C charge/discharge current. All the cells were firstly charged to 4.2 V and kept at 4.2 V until the current dropped to 0.02C (23 mA), then the cells were discharged to 3.0 V. 1C rate means the current is 1.15 A. During each cycle, the cells were also operated in a constant current–constant voltage (CC–CV) charge mode and kept at 4.2 V until the current

was less than 0.02C (23 mA), then underwent a constant current (CC) discharge until its discharge capacity was 30% of the initial capacity. All the rest time between charge and discharge was two minutes.

During the cycling tests, the real capacity of each cell was verified every 100 cycles by using the procedures described above. When the actual capacity fell down to 80% of initial capacity, the cell came to its end of lifetime. To verify the aging mechanisms under different test rates were the same or not, the cells at the capacity retention of 95%, 90%, 85% and 80% ($\pm 0.2\%$) were dismantled and investigated. In order to get an accurate given capacity retention, when the capacity of the full cell decayed close to the preset value, the test procedure was changed to the test of capacity check, so the last “100 cycling” sometimes was less than 100 cycles. Under each cycling condition, at least five cells were conducted to ensure the facticity of the test results, and at least two cells decayed to the capacity retention of 80%. The five cells compared with each other, if one performed differently from the common degradation condition, another one or two cells should be tested. Electrochemical impedance spectroscopy (EIS) tests at discharge state were carried out before dismantling the cells with an AC amplitude of 5 mV over a frequency range from 20 kHz to 5 mHz. The fresh and the aged cells were dismantled until the open circuit voltage was stable and not changing in one day.

The cells were dismantled at discharged state in a glove box filled with pure argon (<1 ppm H₂O, <10 ppm O₂), and each electrode was rinsed with dimethyl carbonate (DMC) in order to extract the lithium salt and then dried at room temperature. XRD measurements of electrode active materials (electrode near the center of the jelly roll) were carried out on a D/max- γ B diffractometer with CuK α radiation, and the surface morphologies of the electrodes were observed by SEM.

Electrochemical tests were done on the fresh and the aged electrodes obtained from the dismantled cells. One side of the coating was rubbed off of the current collector using a cotton-based tissue soaked in 1-methyl-2-pyrolidinone (NMP) to dissolve the polyvinylidene fluoride (PVDF) binder. To minimize the material damage, the electrode was placed on a glass mirror. After the treatment, electrodes with the active material on one side were cut to rounds with a diameter of 14 mm, rinsed twice using DMC, and then dried in vacuum for 1 h without heating. The coin cells underwent a series of tests including residual capacity checkout and low-rate capacity measurement. All the tests were conducted in the test room whose temperature was controlled at 25 °C \pm 2 °C by air-condition and monitored by thermocouple.

3. Results and discussion

3.1. Capacity fade

The capacity retentions of the cells with the cycling time at different charge/discharge rates (0.6C, 1.2C, 1.5C, 1.8C, 2.4C, 3.0C) are shown in Fig. 1. All data are normalized in view of the unequal initial capacities. With cycling, all the cells undergo capacity fade. It shows that as the increase of the charge/discharge rate, the degradation is gradually aggravating compared to the 0.6C. When the rate changes from 0.6C to 1.2C, the effect of accelerating is especially remarkable. However, when the rate exceeds 1.5C, the capacity retention plots are almost constant, the degradation of the full cell under 2.4C or 3.0C is even a little slower than the condition under 1.5C. This may be because that CC time is short under the large rates (140 s for 1.8C, 67 s for 2.4C, 20 s for 3.0C at the beginning of cycling, and the CC time is shortened during cycling),

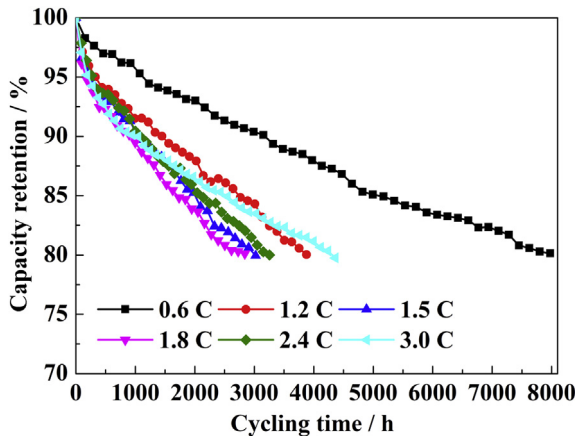


Fig. 1. Normalized capacities as a function of cycling time at different rates (0.6C, 1.2C, 1.5C, 1.8C, 2.4C, 3.0C).

which cannot generate lumping impact on the cells. Meanwhile, the charging time of CV is quite long which current value is similar to the situation of 0.6C. The short CC time is caused by the large polarization under the high rate tests. In addition, the actual voltage applied to the cell is decreased as the rate increases due to the polarization. So, in fact the potential of the cathode under high rate is lower than that under 0.6C. As the charge cut-off voltage reduces, the degradation of the full cell becomes slow [12,33]. That is to say, with the effect of the shorter CC time and the lower voltage during CV process, the fade in capacity under 2.4C and 3.0C rate shows slow.

For the LiCoO₂ material, the time of CV charge stage is quite long, especially under the high rate, which is shown in Fig. 2 (a). Under our test condition, the use range of the capacity is between 100% SOC and 70% SOC, and this means that the 30% capacity is mainly charged during the CV process. So, in this case, the accelerated rate is limited to a low range. When the charge/discharge rate is high, the effect of the high rate is not as distinct as we think. Therefore, even the rate of charge/discharge increases over 1.5C, the effect of acceleration is nearly invariant. A slight fluctuation in capacity observed during cycling is caused by the slight instability of the temperature.

The first charge/discharge profiles of 30% DOD at different test rates and the change of discharge cut-off voltage with the cycling time are shown in Fig. 2. In Fig. 2(a), at the beginning of the charge and discharge steps, there is a rapid voltage change which is attributed to the polarization. Fig. 2(a) presents that as the increasing of the charge/discharge rate, the charge voltage rises and the discharge voltage decreases, illustrating the incremental of polarization in the full cell system. As a result, the interval of SOC which is actually used in tests slides gradually. Fig. 2(b) indicates that the polarization increases gradually during cycling, especially for the high rate tests.

Fig. 3 (a) shows the charge/discharge profiles of the cells when their capacity retentions reach to 80% at different test rates. It can be seen that the curves are almost accordant when the test rate is less than 2.4C although the cells undergo different aging tests. However, compared to others, the charge plain is higher and the discharge plain is lower when the rate is 3.0C. It is illustrated that polarization in the cell increases markedly at the rate of 3.0C. Fig. 3(b) is the result of the EIS tests of 0.6C rate and 3.0C rate when the capacity retention is 80%. The increment impedance also demonstrates that the polarization at 3.0C rate is high.

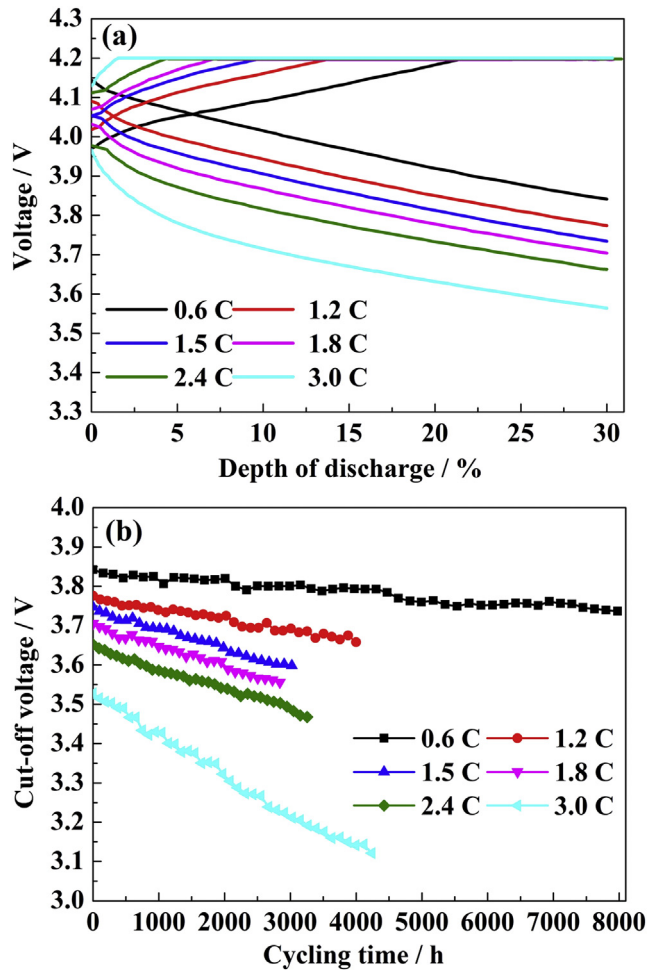


Fig. 2. (a) The first charge/discharge profiles of 30% DOD and (b) the discharge cut-off voltage profiles with the cycling time.

3.2. Morphology of the electrodes (SEM)

Changes in the electrode interface after cycling are studied carefully by observing SEM of the electrode surfaces. Fig. 4 presents the surface morphology of anodes disassembled from the fresh and the aged cells at the four capacity retentions of the 1.2C rate. As for the MCMB anode, it is generally known that the SEI films are generated on the surface of the anode in the first charge, whose nature affects the performance of lithium ion batteries [13]. Fig. 4(a) shows the MCMB particle of the fresh cell which surface is fluffy. Fig. 4(b)–(e) are the MCMB surface morphologies of the samples at the capacity retention of 95%, 90%, 85% and 80% respectively when the rate is 1.2C. It is obvious that there is a layer of the membraniform substance on the surface of the particle, and as the aging of the full cell, the membraniform substance gradually increases. In addition, there are some white protuberances on the surface of the anode, and Fig. 4(f) is the magnified image of the protuberance. It can be seen that the protuberance is generated from the anode surface, not adsorbed on the anode surface, which indicates that it is the constituent of the SEI film and grows as the decay of the full cell. The other samples at dismantling capacity retentions are almost similar and the membraniform substance gradually increases as well with the fade of capacity. However, for the LiCoO₂ electrode, the surface morphology is almost unchanged by the observation of SEM.

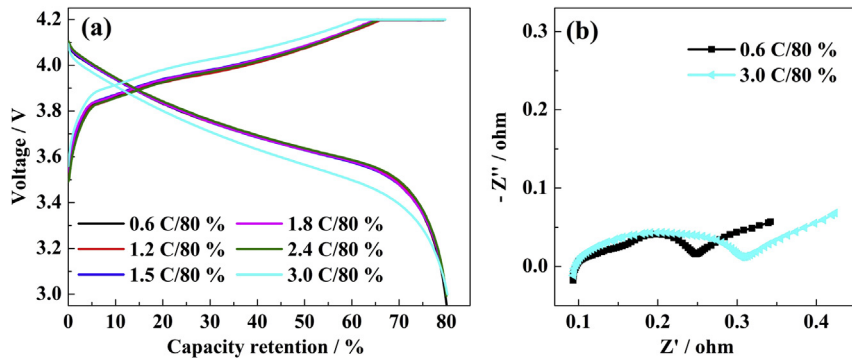


Fig. 3. (a) Charge and discharge profiles and (b) EIS profiles when capacity retentions reach 80% at different test rates.

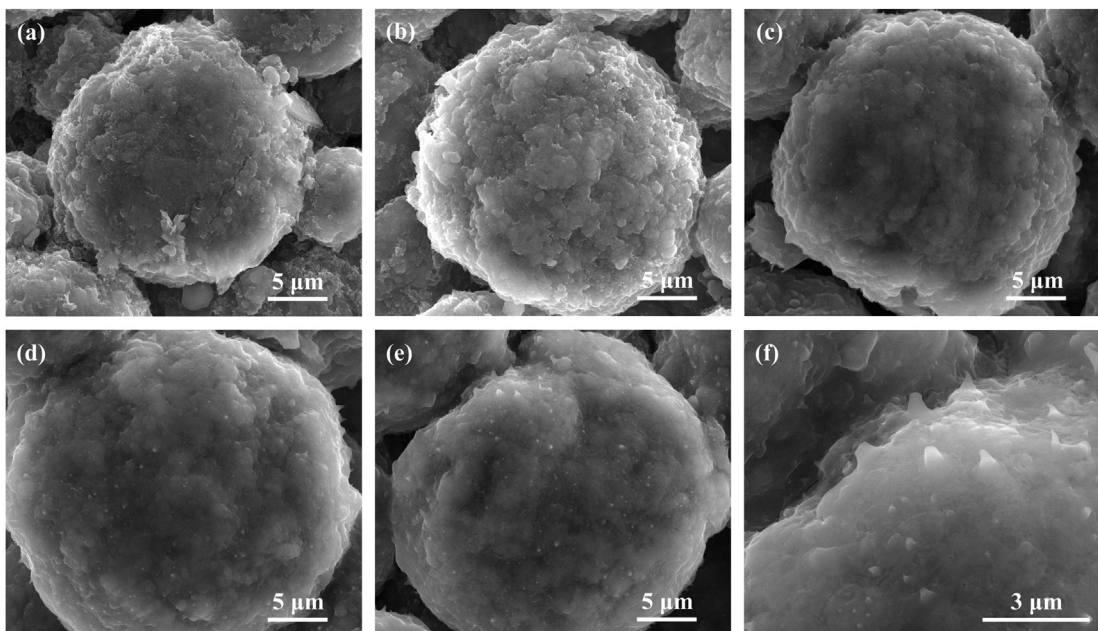


Fig. 4. SEM images of the MCMB electrodes recovered from (a) the fresh cell, (b)–(e) the aged cells of 1.2C/95%, 1.2C/90%, 1.2C/85%, 1.2C/80% and (f) the magnified image of the protuberance on the anode recovered from the aged cell of 1.2C/80%.

3.3. XRD measurements

Fig. 5(a) shows the XRD patterns of the LiCoO₂ electrodes recovered from the fresh and the aged cells of 0.6C rate. There is no significant difference among the XRD patterns, and only the peaks of LiCoO₂ are detected. The diffraction peaks of the aged LiCoO₂ electrodes have the same angular positions as those of the fresh electrode. The difference between patterns is a slight broadening of the peaks. The values of full-width at half-maximum (FWHM) of the (003) for each cathode at different capacity retentions are presented in Table 1. Such a broadening may result from a decrease in the crystallite dimension or from strains within the crystallites themselves [34]. In addition, the height ratios of (006) peak to (012) peak and (018) peak to (110) peak are declined, and the values are listed in Table 1. This also indicates that the structure of LiCoO₂ degrades slightly [30]. Therefore, it is demonstrated that cycling of the cathode does not consequentially lead to the bulk phase transition, but can give rise to significant modifications in the micro-structure, including stress and crystallite [6]. The structures of the LiCoO₂ obtained from other test rates are similar to that under 0.6C. Fig. 5(b) shows the MCMB electrodes from the fresh cell and the

aged cells with the capacity retention of 80%. Since there are no significant changes in the XRD patterns, the structures of anodes under different accelerated rates are nearly not changed. Therefore, the deterioration of the anode is mainly attributed to SEI film [35].

3.4. Half-cell tests

To understand better the capacity fade of full cells under different accelerated aging tests, half-cell studies (i.e., Li/LiCoO₂ and Li/MCMB cells) are performed on both fresh and aged electrodes. Residual and intrinsic (reversible) capacities are measured in both cases. For the LiCoO₂ cathode, the residual capacity corresponds to the x in $\text{Li}_{1-x}\text{CoO}_2$. Namely, there are not enough lithium ions to insert into the $\text{Li}_{1-x}\text{CoO}_2$ when the full cell discharges to 3.0 V. This is because that the active lithium is consumed in the full cell system. The most common causes of irreversible lithium ion consumption are the formation and the development of the SEI film during intercalation at the anode and the decomposition of the electrolyte [14]. Meanwhile some of the lithium ions cannot insert into the cathode due to the limit of polarization. In other words, there are some lithium ions left in the anode owing to the high

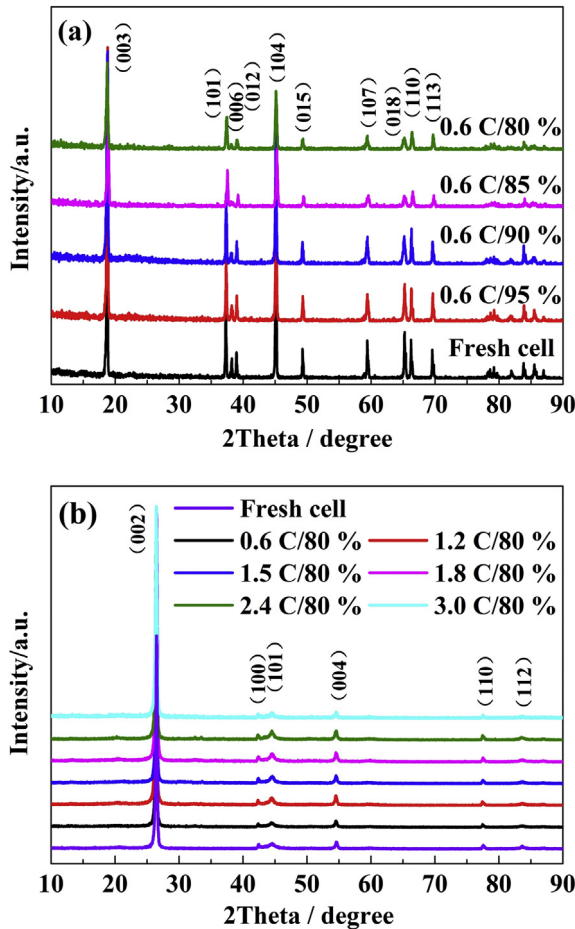


Fig. 5. XRD patterns of the (a) LiCoO₂ electrodes recovered from the fresh cell and the aged cells of 0.6C/95%, 0.6C/90%, 0.6C/85%, 0.6C/80% and (b) MCMB electrodes recovered from the fresh cell and the aged cells at the capacity retention of 80% under different charge/discharge rates.

polarization leading the cell voltage down to the cut-off voltage. For the negative MCMB electrode, the residual capacity corresponds to the amount of lithium left in anode when the full cell is fully discharged. The intrinsic (reversible) capacity is related to the electrode itself, it reflects the intrinsic performance of the electrode, including structure, electric contact between active particles and conductive agent, as well as the current collector. For the anode, the formation and damage of the SEI film is the critical factor to affect its performance [13].

In order to check the intrinsic performance of the cathode and the anode material, low-rate capacity measurements are conducted. For Li/LiCoO₂, the rate is 0.1C and the voltage range is 3.0 V–4.2 V. For Li/MCMB, the rate is 0.05C and the voltage range is 0.01 V–1.5 V. As the inferior rate performance of the MCMB material itself, in order to reflect the intrinsic performance of the MCMB anode, the test rate is lower than the LiCoO₂ cathode. Fig. 6 shows the discharge capacity retention ratios of the 3rd formation

cycle of LiCoO₂ and MCMB electrodes which are recovered from the fresh cell and the aged cells under different cycle rates. The curve shows that as degradation of the full cell, the intrinsic capacity reduces gradually. However, whether the cathode or the anode, the decay of the intrinsic performance is less than the degradation of full cell, and the performance of cathode is better than the anode during the whole test process. Therefore, we should include other factors to clarify the reasons for the decrease in the cell capacity. The decay of intrinsic performance is mainly due to the structural degradation, particle isolation, electrode delamination, loss of electrical contact within the porous electrode and passive films at the active particle surface. When the accelerated rate does not exceed 1.5C, the capacity retention of LiCoO₂ electrode is almost consistent. The capacity retention increases as the test rate rises from 1.8C to 3.0C. For MCMB electrode, the anode capacity retention at the test rate of 3.0C is better than the other groups which are almost consistent. It is illustrated that when the test rate exceeds 1.5C, the aging process of the intrinsic performance of the cathode becomes slower as the rate increases, which means that the aging mechanism is different from the standard test procedure (0.6C). When the test current is higher than a certain value, the rate determining step can be changed from electrochemical step to diffusion step [36]. That is to say, reaction speed is larger than the diffusion speed when the charge/discharge current is high. Due to the high polarization under the high rate, the electrochemical reaction mainly happens on the surface of the electrode, so when the full cell discharges to the cut-off voltage, some inner active material cannot participate in the electrochemical reaction. This explains that the intrinsic performance of electrodes from aged cells changes a little when the rate is higher than 1.5C.

3.4.1. Residual capacity

Here, the prepared anode capacity was sufficiently higher than (about 14%) the cathode capacity to prevent lithium metal plating in the charge state. The measured result of the half-cell also suggests that the anode capacity is much more than the cathode capacity even though the full cell decays to 80% of the initial capacity (i.e., the anode capacity is 4.3088 mAh and the cathode capacity is 3.7891 mAh at the capacity retention of 80% when the test rate is 1.5C). The ratio of the anode/cathode capacity is higher than the projected value, for the actual anode specific capacity is higher than the designed value. As a result, the capacity is limited by the cathode, and the decay of the cathode is one of the main reasons for the fade of the full cell. Fig. 6 shows that degradation of the cathode intrinsic performance is less than the fade in full cell. That is to say, there are some other reasons causing the decay in the full cell. It is found that the residual capacity of the cathode and the anode increases gradually with the aging of the full cell for all test rates. The residual capacities obtained from one electrode of the full cell are usually different, indicating that the state of electrode is uneven. When the full cell is discharged to the cut-off voltage, there are some active materials not participating in the intercalation/deintercalation reaction, and presenting diverse residual capacities. The residual capacities used in the study are mean values of four test samples. For the cathode, the residual capacity is caused by consuming active lithium. When the full cell reaches to the discharge cut-off voltage, some lithium vacancies in the cathode cannot be inserted. Therefore the effective potential window is shortened by the residual capacity.

A representation of cell imbalance of the fresh cell is constructed and presented in Fig. 7 (a). For the fresh cell, the intrinsic capacity of the cathode is 4.0357 mAh, and the residual capacity is 0.3715 mAh, about 9.2% of the intrinsic capacity. For the anode, the intrinsic capacity is 4.9350 mAh, and the residual capacity is 0.0273 mAh, about 0.6%. The difference value of the open circuit voltage between

Table 1

FWHM of the (003) peak, the ratios of (006)/(012) and (018)/(110) for each cathode material obtained from the fresh and aged cells under 0.6C.

	FWHM	(006)/(012)	(018)/(110)
Fresh cell	0.178	0.72	1.25
0.6C/95%	0.204	0.54	0.92
0.6C/90%	0.250	0.42	0.77
0.6C/85%	0.278	0.33	0.62
0.6C/80%	0.288	0.32	0.57

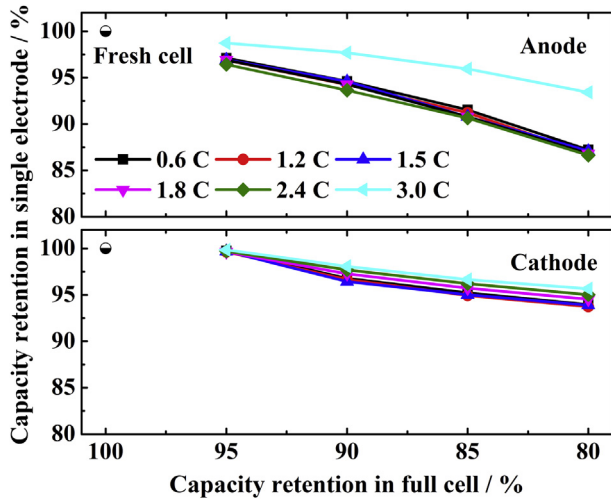


Fig. 6. Discharge capacity retention ratios of the 3rd formation cycle measured at 0.1C and 25 °C of LiCoO₂ and at 0.05C and 25 °C of MCMB electrodes recovered from fresh cell and cells aged under different cycle rates.

the positive half-cell and the negative half-cell is about 3.0 V, which is equal to the cut-off voltage of the full cell, that is to say, the polarization can be ignored. In Fig. 7(a), the irreversible capacity is caused by initial formation process of the full cell, and for the

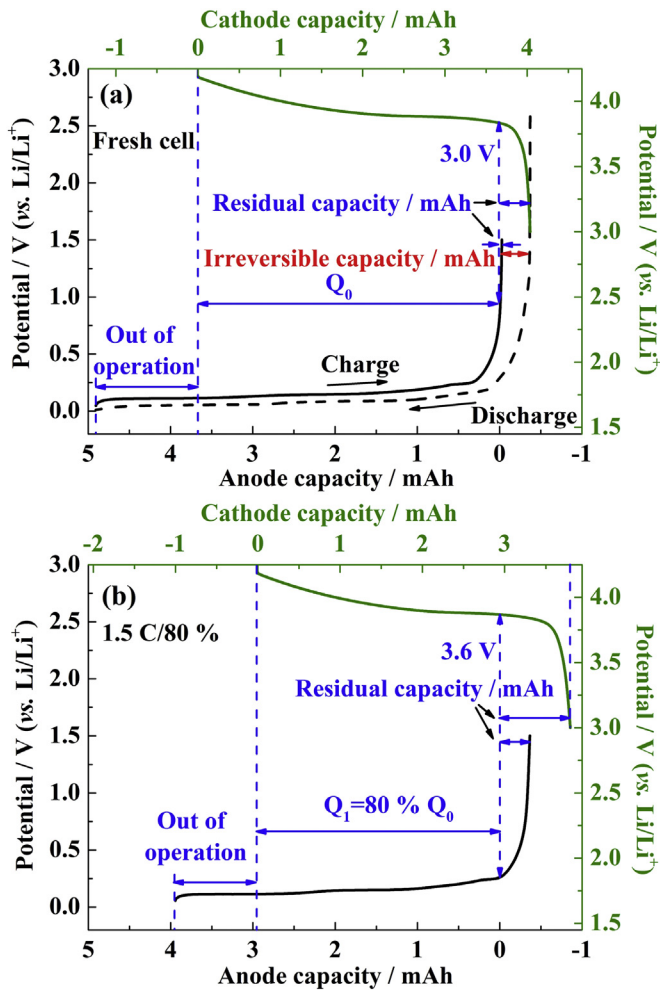


Fig. 7. Potential profiles during discharge of the LiCoO₂/MCMB cells: (a) fresh cell, (b) the aged cell of 1.5C/80%.

anode, the part that is out of operation does not participate in the insert/deinsert reaction, which is attributed to the excess anode capacity comparing to the cathode. As the initial capacities of the full cells are not consistent, we definite the normalized coefficient by formula (1) to normalize the test results to compare the aging factors of the full cells by half-cell tests.

$$\text{normalized coefficient} = \frac{C_{\text{fresh}}^0}{C_{\text{aging}}^0} \quad (1)$$

Where the C_{fresh}^0 is the initial capacity of the fresh cell, the C_{aging}^0 is the initial capacity of the aged cell. For the test results of the half-cells, the residual capacity and the intrinsic capacity are conducted by multiplying the normalized coefficient. After normalizing, the active material loading per unit area is insured a constant. As a consequence, the normalized results can be used to calculate the decay ratio of the full cell.

In Fig. 7(b), for the aged full cell of 1.5C/80%, the intrinsic capacity of the cathode is 3.7891 mAh, and the residual capacity is 0.8576 mAh which is about 22.6% of the intrinsic capacity. Meanwhile the residual capacity of the anode cannot be ignored, and it is about 42.1% of the cathode residual capacity. Here, the cell is operated within the effective range of capacity which is between the two dash straight lines, and the effective capacity Q_1 corresponds to the actual capacity of the full cell. So the factors that affect the aging of the full cell are the degradation of the reversible specific capacity of LiCoO₂ cathode, the consuming of the active lithium irreversibly and the polarization of the full cell. Similar conclusions have been already reported for LiFePO₄/graphite full cell system [26,37] and LiMn₂O₄/LiNi_{0.8}Co_{0.2}Al_{0.05}O₂(8/2)/graphite full cell system [23], suggesting that the consumption of active lithium causes the emerging of the cell imbalance. However, the conclusions above do not take the polarization in consideration in the full cell system, for the cells are discharged by constant voltage before dismantling.

The other test results are summarized in Fig. 8. It shows the reversible capacities and the residual capacities of the electrode materials as well as the effective ranges between the cathode and the anode under different accelerated rates. Here, the residual capacity is under zero, and the differences are hard to distinguish among the groups. In the LiFePO₄/graphite system, the decay in the cathode capacity is ignored [26,37]. However, in the LiCoO₂/MCMB system, the decay of the cathode must be taken account of. So the ratio of the cathode fade must be calculated.

It is assumed that there is no loss of active material due to electrode degradation in the half-cell analyses of both LiCoO₂ and MCMB electrodes, and the coating areas of active materials in different cells are almost equal. We use the formula (2) to calculate the fade of the full cell. In order to distinguish the each influence factor, the formula (3), (4), (5) are applied to evaluate the fade of the cathode, the loss of active lithium and the effect of polarization respectively.

$$\text{calculative capacity fade} = 1 - \frac{(C_{\text{rev}} - C_{\text{res}})_{\text{aging}}}{(C_{\text{rev}} - C_{\text{res}})_{\text{fresh}}} \quad (2)$$

$$\text{calculative cathode capacity fade} = \frac{(C_{\text{fresh}} - C_{\text{aging}})_{\text{rev}}}{(C_{\text{rev}} - C_{\text{res}})_{\text{fresh}}} \quad (3)$$

calculative irreversible lithium accumulation

$$= \frac{(C_{\text{aging}} - C_{\text{fresh}})_{\text{res}} - (A_{\text{aging}} - A_{\text{fresh}})_{\text{res}}}{(C_{\text{rev}} - C_{\text{res}})_{\text{fresh}}} \quad (4)$$

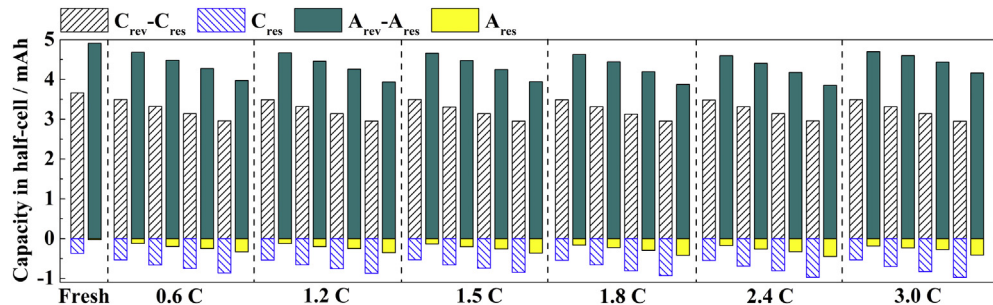


Fig. 8. The reversible capacities and the residual capacities of the electrode materials and the effective ranges between the cathode and the anode (every two columns from left to right between two vertical dash lines correspond to actual capacity retentions which are 95%, 90%, 85%, 80% respectively at each test rate, C_{rev} and C_{res} mean the reversible and the residual capacity of cathode, A_{rev} and A_{res} mean the reversible and the residual capacity of anode respectively).

$$\text{calculative polarization fade} = \frac{(A_{aging} - A_{fresh})_{res}}{(C_{rev} - C_{res})_{fresh}} \quad (5)$$

Where C_{rev} and C_{res} mean the reversible and the residual capacity of cathode, A_{rev} and A_{res} mean the reversible and the residual capacity of anode respectively. The calculative results of the 24 aged cells are listed in Fig. 9. The calculative value is a little smaller than the actual capacity fade since leaving the loss of the active materials out of consideration. But the phenomenon of losing active material actually exists due to electrode degradation. That is to say, the error of the calculative value is caused by the capacity which is generated from the lost active materials. Fig. 9 shows that the consumption of active lithium which contains irreversible lithium accumulation and the lithium left in anode due to polarization is the dominant factor to cause the fade in full cell especially for the initial stage of cycling. Under the same test rate, with the degradation of the full cell, decay of the cathode reversible capacity increases distinctly. So, the proportion of the consumption of active lithium decreases relatively. When the accelerated rate is larger than or equal to 1.8C, the effect of polarization increases, and the proportion of decay in cathode reduces markedly. So, suitable shelf time between charge and discharge to reach the concentration equilibrium is an effective way to improve the capacity of the full cell. Based on the above analysis, 1.5C is suggested to the critical value of the accelerated rate for the specific state. If the active lithium is totally consumed on the anode, the detection of lithium element in the anode will be consistent to the cathode residual capacity. Then, the lithium content is quantitatively analyzed by inductively coupled plasma optical emission spectroscopy (ICP-OES).

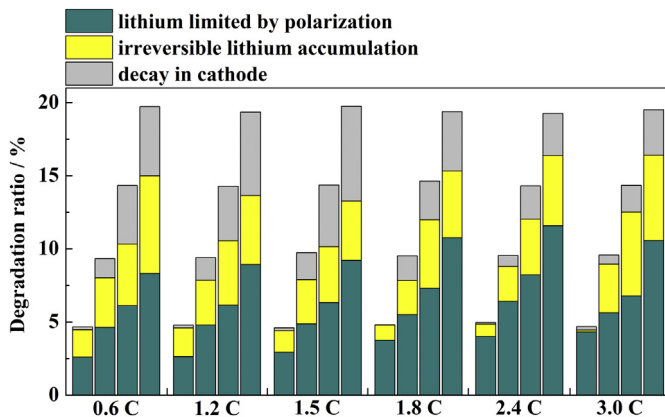


Fig. 9. Ratios of the three aging factors under different conditions (the value of each column is calculated upon half-cell tests, columns from left to right in fours correspond to actual decay ratios which are 5%, 10%, 15%, 20% respectively at each test rate).

3.4.2. Validation of accumulated lithium in anode by ICP-OES

Through the above analysis, we assume that the residual capacity in cathode is caused by the consumption of active lithium in anode. If the assume is right, the content of lithium in the anode would correspond to the amount of lithium calculated by the cathode residual capacity. The test anodes are obtained from the dismantled cells including the fresh cells, the aged cells at the capacity retention of 95% and 80%. Here, quantified amount of lithium should be attributed to electrochemical inactive lithium compounds such as the compositions of SEI film and the active lithium remaining in the anode which is calculated by the anode residual capacity. The tested results and the calculated values of cathode residual capacities are listed in Fig. 10. The illustration shows the ratio of the actual to the calculated value. The ratio is almost 1, illustrating that the lithium in anode totally comes from cathode materials. In addition, the lithium content from the anode increases as the aging of the full cell. The residual capacity of the anode also increases during the aging process.

In order to assess the evolution of the SEI film by the lithium content, we have to subtract the content of the active lithium remaining in the anode from total lithium content in the anode tested by the ICP. For the anode of the fresh cell, one rounded electrode of the half-cell contains 7.1 μ g active lithium caused by polarization and 93.7 μ g inactive lithium from the SEI film. Respect to the cathode, the 7.1 μ g active lithium and the 93.7 μ g inactive lithium account for 0.7% and 9.9% percents of the lithium content calculated by the cathode capacity which is actually used in the cathode (corresponding to $C_{rev} - C_{res}$), respectively. The other

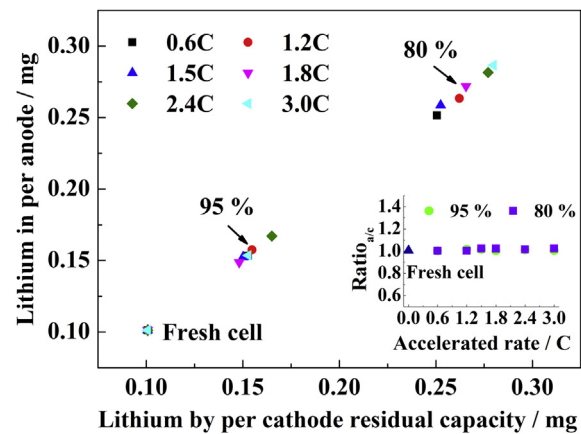


Fig. 10. The relationship between the lithium content calculated by cathode residual capacity and the lithium content of anode in each rounded electrode of the half-cell by ICP-OES.

Table 2

The contents of the active lithium left in anode and inactive lithium of SEI film at different conditions.

Lithium content/μg	0.6C	1.2C	1.5C	1.8C	2.4C	3.0C
95% Q_0						
Active lithium left in anode	31.8	32.1	35	42.8	45.2	48.1
Inactive lithium of SEI film	120.8	122.7	115.2	105.3	119.8	104.7
80% Q_0						
Active lithium left in anode	86.2	92	94.7	109.4	117.2	107.5 ^a
Inactive lithium of SEI film	164.4	170.2	157.8	156.2	159.8	172.4 ^a

^a The values of active lithium and inactive lithium content do not change regularly, and this is because of the test conditions and the characteristic of LiCoO₂ material.

results are listed in Table 2. In addition, the increase of the inactive lithium which is caused by irreversible lithium accumulation indicates that the SEI film is thickened with the degradation of the full cell, but the consuming of the active lithium irreversibly in the initial formation process still accounts for a significant proportion. As discussed in the part 3.1, because of the test conditions and the characteristic of LiCoO₂ material, the effect of the high rate is not as distinct as we think. So, the test results of the active and the inactive lithium content do not change regularly. However, the purpose of the discussion about the active and the inactive lithium content is to explain the effect of the irreversible consumption of the active lithium in the initial formation process. The increase of the active lithium limited by polarization is higher than that of the inactive lithium content as the aging of the full cell, indicating that the effect of the polarization is a little larger than the development of the SEI film. To reduce the effect of polarization in the full cell, we can extend the rest time during use and decrease the applied current.

4. Conclusion

This study presents the aging mechanism of LiCoO₂/MCMB full cell under the different rates (0.6C, 1.2C, 1.5C, 1.8C, 2.4C, 3.0C) and obtains the optimal accelerated rate 1.5C by comparing all the aging processes for the specific state. XRD results show a slight structural degradation in the LiCoO₂ electrode during the accelerated aging tests, and this corresponds with the cathode reversible capacity from the half-cell test results. There is no obvious structural change in MCMB material as the decay of the full cell. The decay in cathode and cell imbalance caused by the loss of active lithium irreversibly and the polarization in the full cell dominate the degradation during cycling. Furthermore, the effect of the active lithium increases as the accelerated rate becomes higher. The proportions of effects by the above three factors are evaluated exactly. The lithium content in the anode tested by ICP-OES is equal to the value of calculated x in the Li_{1-x}CoO₂, indicating that the active lithium is totally from LiCoO₂. The accumulation of lithium by development of the SEI film is less than the amount of lithium left in anode due to the polarization, indicating that the polarization is a significant issue. That is to say, the development of the SEI film during cycling is slow.

Acknowledgments

This work is funded by the National High Technology Research and Development Program (863 Program) of China (No. 2012AA110203).

References

- [1] J.B. Goodenough, Y. Kim, *Chem. Mater.* 22 (2010) 587–603.
- [2] M. Ecker, J.B. Gerschler, J. Vogel, S. Käbitz, F. Hust, P. Dechent, D.U. Sauer, *J. Power Sources* 215 (2012) 248–257.
- [3] C. Delacourt, M. Safari, *J. Electrochem. Soc.* 159 (2012) A1283–A1291.
- [4] M. Broussely, S. Herreyre, P. Biensan, P. Kasztejna, K. Nechev, R.J. Staniewicz, *J. Power Sources* 97–98 (2001) 13–21.
- [5] T. Yoshida, M. Takahashi, S. Morikawa, C. Ihara, H. Katsukawa, T. Shiratsuchi, J.-i. Yamaki, *J. Electrochem. Soc.* 153 (2006) A576–A582.
- [6] J. Li, J. Zhang, X. Zhang, C. Yang, N. Xu, B. Xia, *Electrochim. Acta* 55 (2010) 927–934.
- [7] J. Belt, V. Utgikar, I. Bloom, *J. Power Sources* 196 (2011) 10213–10221.
- [8] R.G. Jungst, G. Nagasubramanian, H.L. Case, B.Y. Liaw, A. Urbina, T.L. Paez, D.H. Doughty, *J. Power Sources* 119–121 (2003) 870–873.
- [9] Q. Zhang, R.E. White, *J. Power Sources* 173 (2007) 990–997.
- [10] K. Takei, K. Kumai, Y. Kobayashi, H. Miyashiro, N. Terada, T. Iwahori, T. Tanaka, *J. Power Sources* 97–98 (2001) 697–701.
- [11] M. Uno, K. Tanaka, *IEEE Trans. Ind. Electron.* 59 (2012) 4704–4712.
- [12] S.S. Choi, H.S. Lim, *J. Power Sources* 111 (2002) 130–136.
- [13] L. Yang, X. Cheng, Y. Ma, S. Lou, Y. Cui, T. Guan, G. Yin, *J. Electrochim. Soc.* 160 (2013) A2093–A2099.
- [14] J. Vetter, P. Novák, M.R. Wagner, C. Veit, K.C. Möller, J.O. Besenhard, M. Winter, M. Wohlfahrt-Mehrens, C. Vogler, A. Hammouche, *J. Power Sources* 147 (2005) 269–281.
- [15] M. Broussely, P. Biensan, F. Bonhomme, P. Blanchard, S. Herreyre, K. Nechev, R.J. Staniewicz, *J. Power Sources* 146 (2005) 90–96.
- [16] Y. Zhang, C.-Y. Wang, X. Tang, *J. Power Sources* 196 (2011) 1513–1520.
- [17] Q. Zhang, R.E. White, *J. Power Sources* 179 (2008) 793–798.
- [18] X. Han, M. Ouyang, L. Lu, J. Li, Y. Zheng, Z. Li, *J. Power Sources* 251 (2014) 38–54.
- [19] T. Tsujikawa, K. Yabuta, T. Matsushita, M. Arakawa, K. Hayashi, *J. Electrochim. Soc.* 158 (2011) A322–A325.
- [20] P. Liu, J. Wang, J. Hicks-Garner, E. Sherman, S. Soukiazian, M. Verbrugge, H. Tataria, J. Musser, P. Finamore, *J. Electrochim. Soc.* 157 (2010) A499–A507.
- [21] M. Dubarry, C. Truchot, B.Y. Liaw, K. Gering, S. Sazhin, D. Jamison, C. Michelbacher, *J. Power Sources* 196 (2011) 10336–10343.
- [22] P. Arora, R.E. White, *J. Electrochim. Soc.* 145 (1998) 3647–3667.
- [23] Y. Kobayashi, T. Kobayashi, K. Shono, Y. Ohno, Y. Mita, H. Miyashiro, *J. Electrochim. Soc.* 160 (2013) A1181–A1186.
- [24] J. Christensen, J. Newman, *J. Electrochim. Soc.* 152 (2005) A818–A829.
- [25] J. Wang, S. Soukiazian, M. Verbrugge, H. Tataria, D. Coates, D. Hall, P. Liu, *J. Power Sources* 196 (2011) 5966–5969.
- [26] M. Safari, C. Delacourt, *J. Electrochim. Soc.* 158 (2011) A1123–A1135.
- [27] D.P. Abraham, S.D. Poppen, A.N. Jansen, J. Liu, D.W. Dees, *Electrochim. Acta* 49 (2004) 4763–4775.
- [28] A.J. Smith, H.M. Dahn, J.C. Burns, J.R. Dahn, *J. Electrochim. Soc.* 159 (2012) A705–A710.
- [29] A. Barré, B. Deguilhem, S. Grolleau, M. Gérard, F. Suard, D. Riu, *J. Power Sources* 241 (2013) 680–689.
- [30] H.P. Zhang, L.J. Fu, Y.P. Wu, H.Q. Wu, *Electrochim. Solid State Lett.* 10 (2007) A283–A285.
- [31] M. Kassem, J. Bernard, R. Revel, S. Pélissier, F. Duclaud, C. Delacourt, *J. Power Sources* 208 (2012) 296–305.
- [32] D. Zhang, B.S. Haran, A. Durairajan, R.E. White, Y. Podrazhansky, B.N. Popov, *J. Power Sources* 91 (2000) 122–129.
- [33] A.J. Smith, N.N. Sinha, J.R. Dahn, *J. Electrochim. Soc.* 160 (2012) A235–A242.
- [34] Y. Ozawa, R. Yazami, B. Fultz, *J. Power Sources* 119–121 (2003) 918–923.
- [35] P. Verma, P. Maire, P. Novák, *Electrochim. Acta* 55 (2010) 6332–6341.
- [36] J. Albery, *Electrode Kinetics*, Clarendon Press, Oxford, 1975. Chap. 4.
- [37] M. Kassem, C. Delacourt, *J. Power Sources* 235 (2013) 159–171.